Charge Distribution and Local Structure of Americium-Bearing Thorium Oxide Solid Solutions

ARTICLE *in* INORGANIC CHEMISTRY · OCTOBER 2012

Impact Factor: 4.76 · DOI: 10.1021/ic301709d · Source: PubMed

4 AUTHORS, INCLUDING:

Damien Prieur
European Commission
33 PUBLICATIONS **365** CITATIONS
SEE PROFILE

Tonya Vitova
Karlsruhe Institute of Technology
36 PUBLICATIONS **212** CITATIONS
SEE PROFILE

Inorganic Chemistry

Article

pubs.acs.org/IC

Charge Distribution and Local Structure of Americium-Bearing Thorium Oxide Solid Solutions

U. Carvajal-Nunez,[†] D. Prieur,*[,†] T. Vitova,[‡] and J. Somers[†]

[†]European Commission, Joint Research Centre, Institute for Transuranium Elements, P.O. Box 2340, D-76125 Karlsruhe, Germany

[‡]Institut für Nukleare Entsorgung (INE), Hermann-von-Helmholtz-Platz, 76344 Eggenstein-Leopoldshafen, Germany

ABSTRACT: The electronical and structural properties of $Th_{0.80}Am_{0.20}O_{2-x}$ materials have been studied by the coupling of X-ray diffraction and X-ray absorption spectroscopy techniques. A substoichiometric fluorite $Th^{IV}_{0.80}Am^{III}_{0.20}O_{1.90}$ solid solution is found following sintering in moisturized $Ar-H_2$. In contrast, heating of this sample in air leads to a nondefective fluorite $Th^{IV}_{0.80}Am^{IV}_{0.20}O_{2.00}$ solid solution. The structures of these solid solution compounds were fully characterized by assessing the interatomic distances, the coordination numbers, and the structural disorder. The effect of the sintering atmosphere on these crystallographical parameters and on the cation valences has been determined and the capability of ThO_2 to accommodate tri- and tetravalent actinides in the fluorite structure assessed.

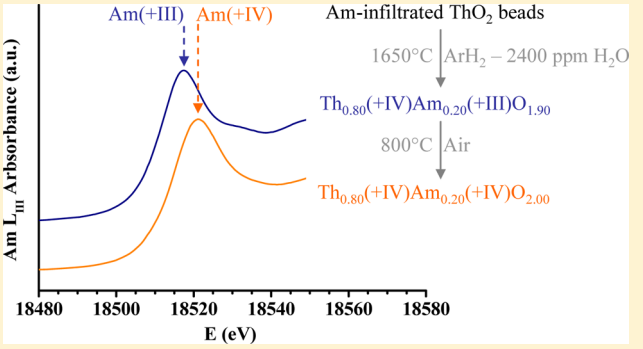

I. INTRODUCTION

Americium (Am) is one of the minor actinides (An) created by neutron capture during the irradiation of UO_2 or $(U,Pu)O_2$ nuclear fuels. Because Am exhibits a high radiotoxicity, its incorporation in oxide materials with a view toward its transmutation in nuclear reactor systems[1,2] for reducing the volume and hazard of radioactive waste is currently considered. Thus, Am is fissioned into short-lived isotopes in neutron flux. Because UO_2 is the most widely used fuel and there is already a strong database on its behavior under neutron irradiation, $U_{1-y}Am_yO_{2-x}$ materials have been studied for this purpose in the past few years[3,4] and test irradiation programs are ongoing.[5,6] Generally, Am contents of about 20% are considered because higher compositions can result in unsatisfactory sodium compatibility. Two recent X-ray absorption spectroscopy (XAS) studies have indicated that Am is strictly Am^{III} in Am-bearing UO_2 solid solutions. However, different results concerning the charge distribution of uranium (U) cations were observed. Vespa et al.[4] have suggested that the oxidation state of uranium is strictly U^{IV}, while Prieur et al.[3] have pointed out the presence of a $U^{IV/V}$ mixed valence, suggesting the occurrence of a compensation charge mechanism during the sintering. Given this discrepancy and potential safety performance implications, it is essential to study the incorporation of Am in a fluorite material without any possibility of charge compensation. ThO_2 is reported as the only stable phase in the Th−O system,[7] implying that thorium (Th) cations have a valence of IV+ in the solid state. Both ThO_2 and AmO_2, just like UO_2, possess a face-centered-cubic lattice of the fluorite-type structure ($Fm\bar{3}m$), so that ThO_2 is an ideal material to investigate the charge distribution. ThO_2 is in its own right a potential nuclear fuel of the future;[8−11] the presented results are therefore interesting for this purpose. Although surrogate systems, i.e., $Th_{1-x}Ln_xO_{2-x/2}$[12,13] and $Ce_{1-x}Ln_xO_{2-x/2}$,[14,15] were recently studied, the structural and electronical properties of $Th_{1-y}Am_yO_{2-x}$ materials have never been reported in the open literature and are described here based on X-ray diffraction (XRD) and XAS studies. These methods probe both long- and short-range order in the material. XAS is a complementary method to assess the local environment around the probed atom and the cation oxidation states. XAS was already used to study the local structure of Am-bearing fluorite materials,[3,4,16−20] $Th_{1-y}U_yO_2$[21] and $Th_{1-y}Pu_xO_2$.[21]

The present investigation was conducted on $Th_{0.80}Am_{0.20}O_{2-x}$ samples that have been sintered either under reducing conditions or in air. The cation valences and structural parameters were determined from XRD and XAS measurements. The dependence of these properties on the sintering conditions is discussed, as is the incorporation of U, plutonium (Pu), and Am in the ThO_2 fluorite structure.

II. EXPERIMENTAL SECTION

II.1. Material Synthesis. The Am-bearing materials were synthesized using a combination of external gelation sol−gel and infiltration methods. The corresponding preparation flowsheet has been described fully in the paper of Vespa et al.[4] This process has been developed at JRC-ITU to ensure dust elimination and liquid waste reduction.[22−24] It basically consists of the infiltration of a ^{241}Am nitrate solution of sol−gel-produced porous ThO_2 beads, which are then

Received: August 3, 2012

   dx.doi.org/10.1021/ic301709d | *Inorg. Chem.* XXXX, XXX, XXX−XXX

thermally treated. The powders were uniaxially pressed to achieve disks, the diameter and height of which are about 6.3 and 1.5 mm, respectively. Two disks were sintered for 8 h at 1650 °C in Ar−H_2. The sintering atmosphere was moisturized with 2400 ppm of H_2O corresponding to an oxygen potential of −384 kJ·mol^{-1} during the sintering dwell period. The heating and cooling rates were 200 °C·h^{-1}.

One of the sintered disks was post-treated under air at 800 °C to achieve the stoichiometric compound. The as-synthesized samples are described in Table 1. XRD and XAS measurements were performed on

Table 1. Compositions and Corresponding Sintering Conditions

composition	sintering conditions
$Th_{0.80}Am_{0.20}O_{1.90}$	sintering at 1650 °C in Ar−H_2 with 2400 ppm of H_2O
$Th_{0.80}Am_{0.20}O_{2.00}$	sintering at 1650 °C in Ar−H_2 with 2400 ppm of H_2O and calcination at 800 °C in Air

the crushed and manually powdered compounds within 1 month after their fabrication to limit the effects of self-irradiation, e.g., increase of the interatomic distances and lattice parameters,[20,25−27] which are induced by the high α activity of ^{241}Am.

II.2. XRD Data Acquisition. XRD analyses were carried at room temperature using a Bragg−Brentano Bruker D8 Advance diffractometer (Cu Kα_1 radiation, 40 kV, and 40 mA) equipped with a Lynxeye linear position-sensitive detector. The powder patterns were recorded using a step size of 0.01973° with an exposure of 4 s across the angular range $10° \leq 2\theta \leq 120°$. Lattice parameters were refined by the Le Bail method using the X'Pert *HighScore Plus* program.

II.3. XAS Data Acquisition and Analysis. XAS data were collected at the INE beamline at the Angströmquelle Karlsruhe (ANKA).[28] A Ge(422) double-crystal monochromator coupled to collimating and focusing rhodium-coated mirrors was used. Data were collected in both transmission and fluorescence modes at Th L_{III} (16300 eV) and Am L_{III} (18510 eV) edges. Fluorescence signals were measured with a four-element germanium solid-state detector. Energy calibration was achieved using yttrium (17038 eV) and zirconium (17998 eV) foils inserted between the second and third ionization chambers. For each X-ray absorption near-edge structure (XANES) measurement, the spectra of the reference foil was systematically collected at the same time. The E_0 values at the absorption edge were taken at the first inflection point using the first zero-crossing value of the second derivative. The energy of white-line maximum at the edge was selected using the first zero-crossing of the first derivative. Several acquisitions (four to six spectra depending on the edge) were performed on the same sample to improve the signal-to-noise ratio.

To determine the oxidation states of Th and Am in the studied samples, XANES spectra at L_{III} edges of reference materials were collected during the same experimental run using the same experimental arrangement. ThO_2 and AmO_2 were used as reference materials for the valence of IV+ of Th and Am, respectively. In addition, the extended X-ray absorption fine structure (EXAFS) measurements of ThO_2 and AmO_2 were analyzed to ensure that stoichiometric compounds were obtained. These results are not presented in this paper, however, because these oxides have already been extensively studied[18,19,29] and our results concur with the reported measurements. The valence of Am and the corresponding molar fractions of Am^{III} and Am^{IV} were determined using the XANES data of Nishi et al. on AmO_2 and Am_2O_3,[18,19] where a difference of 4.0(1) eV between the positions of the white lines of Am_2O_3, i.e., Am^{III}, and AmO_2, i.e., Am^{IV}, was found.[19]

The EXAFS spectra at Th L_{III} and Am L_{III} edges were collected up to 16 and 14 Å^{-1}, respectively. The *ATHENA* software[30] was used to extract EXAFS oscillations from the raw absorption spectra. Experimental EXAFS spectra were Fourier-transformed using a Hanning window over the full k range available at the respective edges. Curve fitting with *ARTEMIS* software[30] was performed in k^3 space. Phases and amplitudes for the interatomic scattering paths were calculated with the ab initio code FEFF8.40.[31] Spherical 7.5 Å clusters of atoms built using the ThO_2 fluorite-type structure (space group $Fm\bar{3}m$) were used for FEFF calculations. This symmetry can be described as a simple cubic packing of anions with cations in the cubic (eight-coordinate) holes. Thus, the cations are surrounded by shells of 8 anions, 12 cations, and 24 anions. For each shell, the coordination numbers were fitted separately. Each cation position in the cluster of atoms was filled with 50% Th and 50% Am. Considering the negligible difference in the calculated amplitude and phase shifts, cation−cation shells were modeled using one metallic backscattering element. In addition, the multiple-scattering paths were also considered in the FEFF calculations. The amplitude factor (S_0^2) was set at 0.90 for Th and Am shells.[32,33] The shift in the threshold energy (ΔE_0) was varied as a global parameter.

III. RESULTS

III.1. XRD Measurements. XRD patterns, presented in Figure 1, show that single-phased ($Fm\bar{3}m$) solid solutions are

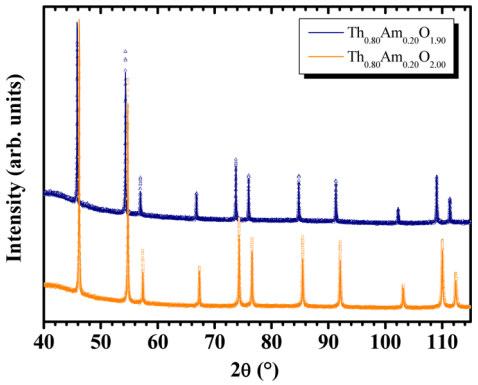

Figure 1. XRD patterns (○, data; —, fit).

achieved for both samples. The refined lattice parameters and, on the basis of these, the calculated interatomic distances are given in Table 2. The lattice parameter of the material sintered

Table 2. Structural Parameters Calculated from the XRD Results

sample	space group	lattice parameter (Å)	Me−O distance (Å)[a]	Me−Me distance (Å)[a]
$Th_{0.80}Am_{0.20}O_{1.90}$	$Fm\bar{3}m$	5.597(1)	2.42(1)	3.96(1)
$Th_{0.80}Am_{0.20}O_{2.00}$	$Fm\bar{3}m$	5.556(1)	2.41(1)	3.94(1)

[a]These distances were calculated from the lattice parameters assessed by XRD.

in air, which is expected to be the dioxide $Th_{0.80}Am_{0.20}O_{2.00}$, is equal to 5.556(1) Å. This is consistent with the value derived from the Vegard's law, i.e., 5.553 Å, based on the lattice parameters of ThO_2 (5.5975 Å[34]) and AmO_2 [5.376(1) Å[35]]. The lattice parameter of $Th_{0.80}Am_{0.20}O_{2-x}$ sintered in moisturized Ar−H_2 is 5.597(1) Å, is higher than that for the corresponding mixed dioxide, and is actually similar to the reported value of ThO_2.[34] As would be expected, this value is also close to the lattice parameter measured for the surrogate $Th_{1-x}Nd_xO_{2-x/2}$ materials.[12] In the reducing conditions under which the sample was prepared, the deviation from the stoichiometry might explain this effect. Thus, the determination of the oxidation states using XANES analysis is therefore useful to confirm this assumption and indeed essential for the determination of the oxidation states themselves.

dx.doi.org/10.1021/ic301709d | Inorg. Chem. XXXX, XXX, XXX−XXX

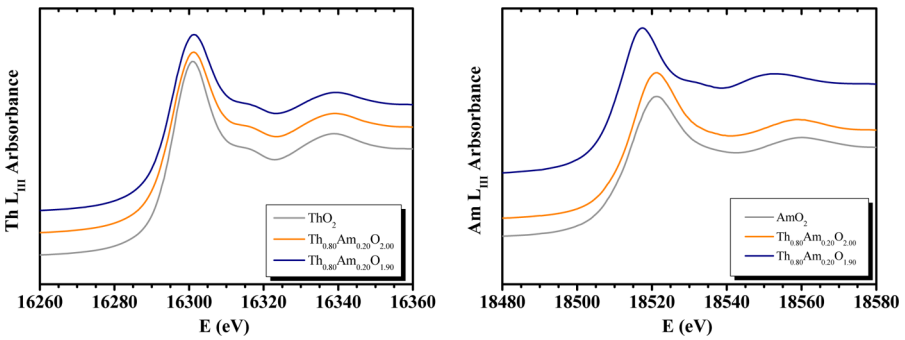

Figure 2. XANES spectra at Th L_{III} and Am L_{III} edges.

Table 3. Energies of the Inflection Point and White Line of the XANES Spectra, Valences of Th and Am Cations, Molar Fractions, and O/M Ratios

			valence		molar fraction (%)			
sample	inflection point (eV)	white line (eV)	Th	Am[a]	Th^{IV}	Am^{III}	Am^{IV}	O/M[b]
			Th L_{III}					
ThO_2	16296.1	16301	4					
$Th_{0.80}Am_{0.20}O_{1.90}$	16295.8	16301.2	4		80			1.90(1)
$Th_{0.80}Am_{0.20}O_{2.00}$	16296.1	16301	4		80			2.00(1)
Am L_{III}								
AmO_2	18513.9	18521.2		4				
$Th_{0.80}Am_{0.20}O_{1.90}$	18510.9	18517.3		4.0(1)		20(1)	0(1)	1.90(1)
$Th_{0.80}Am_{0.20}O_{2.00}$	18513.8	18521.1		3.0(1)		0(1)	20(1)	2.00(1)

[a]The valence was calculated considering a shift of 4 eV between the white lines of AmO_2 and Am_2O_3. [b]The O/M ratios were determined, respecting the structure electroneutrality.

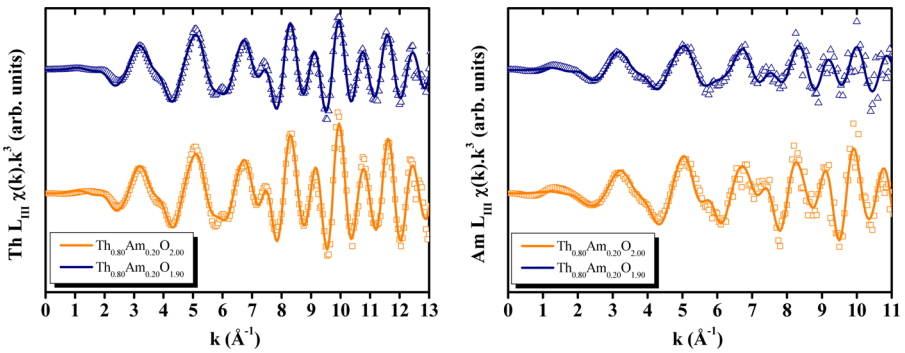

Figure 3. Experimental and fitted EXAFS spectra at Th L_{III} and Am L_{III} edges (○, data; —, fit).

III.2. XANES Results. Th L_{III} and Am L_{III} XANES spectra of the studied samples and the corresponding reference materials are presented in Figure 2. The associated energies of inflection points and white lines directly at the absorption edge are provided in Table 3.

At the Th L_{III} edge, no shift of the white line or inflection point energies is observed for the Am-bearing samples compared to those for the reference material ThO_2. This indicates that the oxidation state of Th cations is equal to IV+ whatever the sintering conditions, as indeed would be expected.

At the Am L_{III} edge, however, the $Th_{0.80}Am_{0.20}O_{2-x}$ sample treated in Ar−H_2 exhibits a shift of 4 eV to lower energies, indicating that Am is reduced to Am^{III}. The $Th_{0.80}Am_{0.20}O_{2-x}$ sample sintered in air exhibits a spectrum similar to that of the reference AmO_2, indicating the presence of Am^{IV}. As explained above in the Experimental Section, the valence of Am can be linearly deduced from the shift of 4.0(1) eV between the white lines of AmO_2 and Am_2O_3, as reported by Nishi et al.[19] The energy shift (ΔE) and the estimated oxidation states derived from these studies are provided in Table 3. As expected, the lowest Am valence is obtained for the more reducing atmosphere, i.e., moisturized Ar−H_2. Thus, Am in $Th_{0.80}Am_{0.20}O_{2-x}$ is strictly present in valence states III+ and IV+ upon sintering under reducing conditions and following an oxidative treatment at 800 °C, respectively. Consequently, the solid solutions can be described as $Th^{IV}_{0.80}Am^{III}_{0.20}O_{1.90}$ and $Th^{IV}_{0.80}Am^{IV}_{0.20}O_{2.00}$ in Ar−H_2 and in air, respectively. It is noteworthy that a total oxidation of Am^{III} to Am^{IV} is achieved by heating the reduced sample in air at 800 °C.

III.3. EXAFS Results. As outlined in the Experimental Section, FEFF calculations were based on spherical 7.5 Å clusters of atoms built using the fluorite-type structure ($Fm\bar{3}m$). Because XRD has indicated that this material is present in a single phase, a single fluorite phase was considered for the FEFF calculations. The EXAFS spectra and their associated Fourier transforms are presented in Figures 3 and 4,

dx.doi.org/10.1021/ic301709d | Inorg. Chem. XXXX, XXX, XXX−XXX

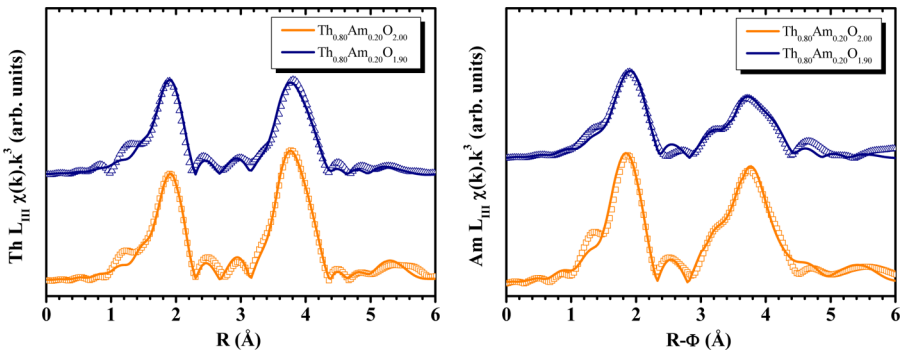

Figure 4. Fourier transforms of experimental and fitted EXAFS spectra at Th L_{III} and Am L_{III} edges (○, data; —, fit).

Table 4. Structural Parameters Calculated by the Fitting of k^3-Weighed EXAFS Spectra

sample	edge	shell	R (Å)	N	σ^2 (Å^2)	R_f (%)	R_{XRD} (Å)
$Th_{0.80}Am_{0.20}O_{1.90}$	Th L_{III} (k range: 2.8−13.2 Å^{-1})	O	2.42(1)	7.9(5)	0.007(1)	1.7	2.42
		Me	3.93(1)	11.8(5)	0.006(1)		3.96
		O	4.59(1)	24(2)	0.010(2)		
	Am L_{III} (k range: 2.9−11.1 Å^{-1})	O	2.41(1)	7.6(5)	0.008(1)	2.2	2.42
		Me	3.94(1)	11.8(5)	0.006(1)		3.96
		O	4.54(1)	24(2)	0.011(1)		
$Th_{0.80}Am_{0.20}O_{2.00}$	Th L_{III}(k range: 2.8−13.2 Å^{-1})	O	2.41(1)	8.1(5)	0.005(1)	1.4	2.41
		Me	3.92(1)	11.9(5)	0.004(1)		3.94
		O	4.58(1)	24(2)	0.008(1)		
	Am L_{III} (k range: 2.9−11.1 Å^{-1})	O	2.36(1)	8.0(5)	0.006(1)	2.1	2.41
		Me	3.93(1)	11.9(5)	0.005(1)		3.94
		O	4.52(1)	24(2)	0.008(1)		

respectively. Immediate inspection of the data shows that there is a significant difference in the periodicity of the oscillations for the Am^{IV}- and Am^{III}-based compounds at the Am L_{III} edge, indicating major structural differences. The data at the Th L_{III} edge are more similar and the differences more subtle. A good agreement between the experimental and fitted data is observed, confirming the validity of the structural models used in the analysis. The structural parameters derived from analysis of the EXAFS data are provided in Table 4.

In the stoichiometric compound, the first Th−O distance is equal to 2.41(1) Å and the second Th−metal (Me) distance is 3.92(1) Å at the Th L_{III} edge. Despite the fact that they are just beyond the experimental error, these interatomic distances are slightly longer in $Th_{0.80}Am_{0.20}O_{1.90}$, as would be expected with the lower O/M ratio. The Th−O first distance is in good agreement with that derived from XRD determination of the lattice parameter (cf. Table 2). At the Am L_{III} edge, no additional Am−Am distances or distances compatible with the Am_2O_3 structure were needed to reproduce the experimental data, confirming the local integration of Am^{III} in the fluorite structure. Note that this is consistent with the results reported recently on $Th_{1-x}Ln_xO_{2-x/2}$[12] and $Ce_{1-x}Ln_xO_{2-x/2}$.[14,36,15] The bond lengths of the first Am−O atoms are equal to 2.36(1) and 2.41(1) Å for $Th_{0.80}Am_{0.20}O_{1.90}$ and $Th_{0.80}Am_{0.20}O_{2.00}$ compounds, respectively. This significant difference is explained by the oxidation states of Am and the corresponding ionic radii, which are $r(Am^{III})$ = 1.09 Å and $r(Am^{IV})$ = 0.95 Å.[37,38] Both Th−Me and Am−Me distances are approximately equal to 3.93(1) Å, which is slightly lower than the Me−Me distance determined from the XRD measurement of the lattice parameters (cf. Table 2). The Am−O third-shell distance decreases slightly when the O/M ratio increases, but again the bond-length difference is just beyond the experimental error. Such a tendency has already been observed in the U−Am−O system.[3]

For the $Th_{0.80}Am_{0.20}O_{2.00}$ sample, the coordination numbers of the Me−O first and third shells are equal to 8.1(5) and 24(2), indicating the absence of oxygen vacancies randomly distributed in the anion sublattice, as would be expected in the stoichiometric dioxide, so that the stoichiometry of this solid solution is consistent with both valences and molar fractions calculated from the XANES results. However, the presence of such defects is suggested in the Me−O first shell of $Th_{0.80}Am_{0.20}O_{1.90}$, where the coordination number is reduced to 7.6(5) around Am (but remains close to 8 around the Th atoms considering the uncertainty), again consistent with the calculated O/M ratio, which indicates a deviation from stoichiometry. In the case of hypostoichiometric oxides, oxygen vacancies are expected to be the dominant defects. For both materials, the coordination value of the Me−Me shell is equal to 11.9(5), indicating that the cation sublattice is not significantly affected by the sintering atmosphere, which would be expected.

Generally, the Debye−Waller factor values are lower for all bond distances in the stoichiometric dioxide sample. This can be caused by the presence of oxygen vacancies in the samples heated in Ar−H_2, which increases the structural disorder of the system.

IV. DISCUSSION

IV.1. Effect of the Sintering Atmosphere. Considering the XRD and XAS results, a substoichiometric fluorite $Th^{IV}_{0.80}Am^{III}_{0.20}O_{1.90}$ solid solution is achieved by sintering at 1650 °C in moisturized Ar−H_2. The respective valences of the Am and Th cations can be understood from the thermodynamical properties of thorium and americium oxides. ThO_2

dx.doi.org/10.1021/ic301709d | Inorg. Chem. XXXX, XXX, XXX−XXX

exhibits a very low oxygen potential, in contrast to AmO_{2-x}.[7,39,40] Consequently, under reducing conditions (moisturized $Ar-H_2$), Am^{IV} is easily reduced while ThO_2 remains stoichiometric. The valence IV+ of Th is an expected result because only the ThO_2 compound is reported as a stable phase in the Th−O system. ThO has only been reported as a metastable species.[7] Regarding the oxidation state of Am, the thermal treatment leads to a total reduction of Am to Am^{III}. Similar results have already been reported in the U−Am−O system for the same Am content.[3,4] The presence of Am^{III}, instead of Am^{IV}, results in the formation of oxygen vacancies distributed in the anion sublattice. The presence of these defects is expected in the case of hypostoichiometric oxides. According to the derived coordination numbers, one can assume that these point defects seem to be located mainly in the Am local environment, which is directly impacted by the reduction of Am^{IV} to Am^{III}. This statement is an assumption because the error in the determination of the coordination number using EXAFS is rarely better than 0.5. For large deviations from stoichiometry, the defects can become nonisolated and start to interact with each other. Thus, an EXAFS study[33] on $U_{1-y}Pu_yO_{2-x}$ has shown that the mixed oxide has a disordered hyperstoichiometric structure with cuboctahedral defects located in the U environment. Such Willis-type defects[41] were not observed in the present work. Finally, it is interesting and important to mention that a single-phase material was achieved when Am^{III} was present. Although this result is consistent by comparison with surrogate systems,[12,14] this is in contrast to a demixing into two substoichiometric fluorite solid solutions observed in $Pu_{0.91}Am_{0.09}O_{2-x}$ samples, which have been fabricated by powder metallurgy and sintered under conditions similar to ours.[42] In the present work, this could indicate that the fluorite structure is stabilized by Th, which constitutes the major cation element of the fluorite matrix and may well be correlated to the low oxygen potential of ThO_2. In contrast, in the $(Pu,Am)O_{2-x}$ system, both cations can be reduced, which could result in a two-phase system when the total O/M ratio decreases.

The heating at 800 °C in air of the fluorite $Th^{IV}_{0.80}Am^{III}_{0.20}O_{1.90}$ solid solution leads to a nondefective fluorite $Th^{IV}_{0.80}Am^{IV}_{0.20}O_{2.00}$ solid solution. In these conditions, the obtained valence IV+ of both Th and Am cations is consistent with the oxygen potentials of ThO_2 and AmO_{2-x}. This indicates that the thermal treatment was sufficient to recover the oxygen vacancies, i.e., to completely oxidize Am^{III} to Am^{IV}. During sintering in $Ar-H_2$, the thermal energy is taken up by densification and diffusion processes. Therefore, in the case of the post-thermal treatment in air, the available thermal energy is mainly devoted to oxygen diffusion. The absence of vacancies in the cation or in the anion sublattice is in agreement with the low values of the Debye−Waller factor derived from EXAFS analysis. Although the local deformation associated with the difference of ionic radii contributes to the total Debye−Waller factor, one can assume that a significant contribution is due to thermal vibrations because all XAS measurements have been performed at room temperature.

In addition, Am−Me and Th−Me distances are very close (3.92 and 3.93 Å, respectively, compared with 3.94 Å, derived from XRD), while there is a very significant difference between Am−O and Th−O (2.41 and 2.36 Å, respectively, compared with 2.41 Å from XRD). This suggests that there is a bimodal distribution of the distances in the first shell, as was previously reported by Hubert et al. in $Th_{1-y}U_yO_{2.00}$ and $Th_{1-y}Pu_yO_{2.00}$.[21] Besides and as discussed in the work of Hubert et al.,[21] a local shortening around the higher An bond length is observed, suggesting that there is no evidence for local clustering of Th or Am in $Th_{0.80}Am_{0.20}O_{2.00}$.

Comparing the EXAFS and XRD data on the Am^{III}- and Am^{IV}-bearing ThO_2 solid solution, one can conclude that the ThO_2 fluorite structure perfectly accommodates the presence of the trivalent cation, as would be expected from previous studies on surrogate systems.[12,14] The difference of the charge distribution obviously leads to a change of interatomic distances, coordination numbers, and structural disorder. Nevertheless, no structural distortion of the cation sublattice, significant local clustering, or demixing is observed, supporting the exceptional stability of the fluorite structure.

IV. 2. Comparison with $Th_{1-y}U_yO_{2.00}$ and $Th_{1-y}Pu_yO_{2.00}$.

The structural parameters of $Th_{0.80}Am_{0.20}O_{2.00}$ determined in this investigation have been compared with those of $Th_{0.80}U_{0.20}O_{2.00}$ and $Th_{0.80}Pu_{0.20}O_{2.00}$ from Hubert et al.[21] The comparison is performed solely for the dioxide solid solutions.

The lattice parameters of $AnO_{2.00}$ and $Th_{0.80}An_{0.20}O_{2.00}$ are presented in Figure 5 as a function of the ionic radii of the 8-fold-coordinated Me^{IV} cations for the An corresponding to U, Pu, and Am. As expected, the lattice parameter of the simple AnO_2 varies linearly with the ionic radius. A similar trend is observed for the lattice parameter in the $Th_{0.80}An_{0.20}O_{2.00}$ solid solutions. It is interesting to note that the slope of the $AnO_{2.00}$ lattice parameter versus the ionic radius is greater than that of $Th_{0.80}An_{0.20}O_{2.00}$, pointing out the geometrical modification induced by the incorporation of a doping cation. The effect is smaller because of the 20% dilution in the solid solution. Figure 6 presents the first Me−O distance of the $Th_{0.80}Me_{0.20}O_{2.00}$ solid solution as a function of the ionic radius of the 8-fold-coordinated Me^{IV} cations (Me = Th, U, Pu, and Am). In agreement with the tendency observed for the lattice parameter, the interatomic distance decreases with a decrease of the ionic radius. The slope of the An−O distances (An = U, Pu, and Am) is higher than that of the Th−O bond lengths in these compounds, as would be expected.

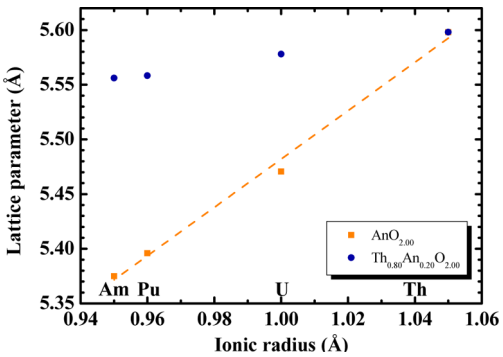

Figure 5. Lattice parameters of $AnO_{2.00}$ and $Th_{0.80}An_{0.20}O_{2.00}$ versus the ionic radii of the 8-fold-coordinated IV+ cations (the dashed lines are given only as a guide; the ionic radii of Shannon et al.[38] and the experimental data of Hubert et al.[21] were considered; An = U, Pu, and Am).

V. CONCLUSION

The charge distribution and local structure of $Th_{0.80}Am_{0.20}O_{2-x}$ and $Th_{0.80}Am_{0.20}O_{2.00}$ were investigated by coupled XRD and XAS measurements. One sample was sintered in moisturized

dx.doi.org/10.1021/ic301709d | Inorg. Chem. XXXX, XXX, XXX−XXX

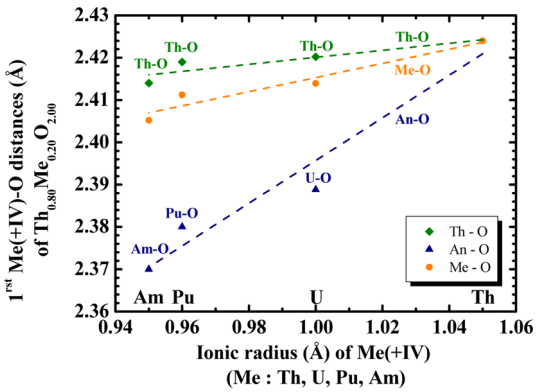

Figure 6. First Me−O distances versus the ionic radii of the 8-fold-coordinated IV+ cations (the dashed lines are given only as a guide; the ionic radii of Shannon et al.[38] and the experimental data of Hubert et al.[21] were considered; Me−O is the weighted average distance; An = U, Pu, and Am).

Ar−H_2, and a substoichiometric fluorite $Th^{IV}_{0.80}Am^{III}_{0.20}O_{1.90}$ solid solution was achieved. Thus, the reducing conditions lead to the total reduction of Am to Am^{III}, giving rise to oxygen vacancies in the anion sublattice. The heating in air of this material leads to the complete oxidation of Am^{III} to Am^{IV} and, consequently, to the formation of a nondefective fluorite $Th^{IV}_{0.80}Am^{IV}_{0.20}O_{2.00}$ solid solution. In a comparison with the previous data on $Th_{0.80}U_{0.20}O_{2.00}$ and $Th_{0.80}Pu_{0.20}O_{2.00}$ materials, it was shown that the fluorite structure perfectly accommodates the presence of various cations. The doping results in a variation of the interatomic distances and lattice parameters, but no evidence for significant clustering of metal elements was found.

AUTHOR INFORMATION

Corresponding Author

*E-mail: dam.prieur@gmail.com. Tel: +49 7247 951 130.

Notes

The authors declare no competing financial interest.

ACKNOWLEDGMENTS

The authors gratefully acknowledge Co Boshoven, Sébastien Gardeur, Herwin Hein, and Patrick Lajarge for sample preparation, Daniel Bouxière and Rachel Eloirdi for the XRD acquisition, and Amir Hein for his advice on the XRD refinement. The authors are grateful to ANKA for the provision of beamtime and Kathy Dardenne for her assistance during the XAS data acquisition.

REFERENCES

(1) Babelot, J.-F.; Conrad, R.; Konings, R. J. M.; Mühling, G.; Salvatores, M.; Vambenepe, G. *J. Alloys Compd.* **1998**, *271−273*, 606−609.

(2) Ogawa, T. *Prog. Nucl. Energy* **2002**, *40*, 539−546.

(3) Prieur, D.; Martin, P. M.; Jankowiak, A.; Gavilan, E.; Scheinost, A. C.; Herlet, N.; Dehaudt, P.; Blanchart, P. *Inorg. Chem.* **2011**, *50*, 12437−12445.

(4) Vespa, M.; Rini, M.; Spino, J.; Vitova, T.; Somers, J. *J. Nucl. Mater.* **2012**, *421*, 80−88.

(5) D'Agata, E.; Hania, P. R.; Bejaoui, S.; Sciolla, C.; Wyatt, T.; Hannink, M. H. C.; Herlet, N.; Jankowiak, A.; Klaassen, F. C.; Bonnerot, J.-M. *Nucl. Eng. Des.* **2011**.

(6) Prieur, D.; Jankowiak, A.; Thibaud, D.; Nathalie, H.; Philippe, D.; Philippe, B. *J. Nucl. Mater.* **2011**, *414*, 503−507.

(7) Guéneau, C.; Chartier, A.; Van Brutzel, L. *Comprehensive Nuclear Materials*; Elsevier: Oxford, U.K., 2012; pp 21−59.

(8) Fourest, B.; Vincent, T.; Lagarde, G.; Hubert, S.; Baudoin, P. *J. Nucl. Mater.* **2000**, *282*, 180−185.

(9) Herring, J. S.; MacDonald, P. E.; Weaver, K. D.; Kullberg, C. *Nucl. Eng. Des.* **2001**, *203*, 65−85.

(10) Hingant, N.; Clavier, N.; Dacheux, N.; Hubert, S.; Barré, N.; Podor, R.; Aranda, L. *Powder Technol.* **2011**, *208*, 454−460.

(11) Hubert, S.; Barthelet, K.; Fourest, B.; Lagarde, G.; Dacheux, N.; Baglan, N. *J. Nucl. Mater.* **2001**, *297*, 206−213.

(12) Horlait, D.; Tocino, F.; Clavier, N.; Dacheux, N.; Szenknect, S. *J. Nucl. Mater.* **2012**, *429*, 237−244.

(13) Horlait, D.; Clavier, N.; Dacheux, N.; Cavalier, R.; Podor, R. *Mater. Res. Bull.* **2012**.

(14) Horlait, D.; Claparède, L.; Clavier, N.; Szenknect, S.; Dacheux, N.; Ravaux, J.; Podor, R. *Inorg. Chem.* **2011**, *50*, 7150−7161.

(15) Claparede, L.; Clavier, N.; Dacheux, N.; Moisy, P.; Podor, R.; Ravaux, J. *Inorg. Chem.* **2011**, *50*, 9059−9072.

(16) Walter, M.; Nästren, C.; Somers, J.; Jardin, R.; Denecke, M. A.; Brendebach, B. *J. Solid State Chem.* **2007**, *180*, 3130−3135.

(17) Martin, P. M.; Belin, R. C.; Valenza, P. J.; Scheinost, A. C. *J. Nucl. Mater.* **2009**, *385*, 126−130.

(18) Nishi, T.; Nakada, M.; Itoh, A.; Suzuki, C.; Hirata, M.; Akabori, M. *J. Nucl. Mater.* **2008**, *374*, 339−343.

(19) Nishi, T.; Nakada, M.; Suzuki, C.; Shibata, H.; Itoh, A.; Akabori, M.; Hirata, M. *J. Nucl. Mater.* **2010**, *401*, 138−142.

(20) Prieur, D.; Martin, P. M.; Lebreton, F.; Delahaye, T.; Jankowiak, A.; Laval, J.-P.; Scheinost, A. C.; Dehaudt, P.; Blanchart, P. *J. Solid State Chem.* **2012**, *194*, 206−211.

(21) Hubert, S.; Purans, J.; Heisbourg, G.; Moisy, P.; Dacheux, N. *Inorg. Chem.* **2006**, *37*, 3887−3894.

(22) Richter, K.; Fernandez, A.; Somers, J. *J. Nucl. Mater.* **1997**, *249*, 121−127.

(23) Fernandez, A.; Richter, K.; Somers, J. *J. Alloys Compd.* **1998**, *271−273*, 616−619.

(24) Fernandez, A.; McGinley, J.; Somers, J.; Walter, M. *J. Nucl. Mater.* **2009**, *392*, 133−138.

(25) Hurtgen, C.; Fuger, J. *Inorg. Nucl. Chem. Lett.* **1977**, *13*, 179−188.

(26) Walter, M.; Somers, J.; Fernandez, A.; Haas, D.; Dardenne, K.; Denecke, M. A. *J. Nucl. Mater.* **2007**, *362*, 343−349.

(27) Prieur, D.; Jankowiak, A.; Roudil, D.; Dubois, S.; Leorier, C.; Herlet, N.; Dehaudt, P.; Laval, J.-P.; Blanchart, P. *J. Nucl. Mater.* **2011**, *411*, 15−19.

(28) Rothe, J.; Butorin, S.; Dardenne, K.; Denecke, M. A.; Kienzler, B.; Löble, M.; Metz, V.; Seibert, A.; Steppert, M.; Vitova, T.; Walther, C.; Geckeis, H. *Rev. Sci. Instrum.* **2012**.

(29) Rothe, J.; Denecke, M. A.; Neck, V.; Müller, R.; Kim, J. I. *Inorg. Chem.* **2002**, *41*, 249−258.

(30) Ravel, B.; Newville, M. *J. Synchrotron Radiat.* **2005**, *12*, 537−541.

(31) Rehr, J. J.; Ankudinov, A.; Zabinsky, S. I. *Catal. Today* **1998**, *39*, 263−269.

(32) Martin, P.; Grandjean, S.; Ripert, M.; Freyss, M.; Blanc, P.; Petit, T. *J. Nucl. Mater.* **2003**, *320*, 138−141.

(33) Martin, P.; Grandjean, S.; Valot, C.; Carlot, G.; Ripert, M.; Blanc, P.; Hennig, C. *J. Alloys Compd.* **2007**, *444−445*, 410−414.

(34) Zachariasen, W. *Phys. Rev.* **1948**, *73*, 1104−1105.

(35) Prieur, D.; Jankowiak, A.; Leorier, C.; Herlet, N.; Donnet, L.; Dehaudt, P.; Maillard, C.; Laval, J.-P.; Blanchart, P. *Powder Technol.* **2011**, *208*, 553−557.

(36) Horlait, D.; Claparède, L.; Clavier, N.; Szenknect, S.; Dacheux, N.; Ravaux, J.; Podor, R. *Inorg. Chem.* **2011**, *50*, 7150−7161.

(37) Shannon, R. D.; Prewitt, C. . *Acta Crystallogr., Sect. B* **1969**, *25*, 925−946.

(38) Shannon, R. D. *Acta Crystallogr., Sect. A* **1976**, *32*, 751−767.

(39) Kinoshita, H.; Setoyama, D.; Saito, Y.; Hirota, M.; Kurosaki, K.; Uno, M.; Yamanaka, S. *J. Chem. Thermodyn.* **2003**, *35*, 719−731.

(40) Thiriet, C.; Konings, R. J. M. *J. Nucl. Mater.* **2003**, *320*, 292−298.
(41) Garrido, F.; Ibberson, R. M.; Nowicki, L.; Willis, B. T. M. *J. Nucl. Mater.* **2003**, *322*, 87−89.
(42) Miwa, S.; Ishi, Y.; Osaka, M. *J. Nucl. Mater.* **2009**, *389*, 402−406.